

Absolute magnitudes and slope parameters for 250,000 asteroids observed by Pan-STARRS PS1 - preliminary results.

P. Vereš^{a,b}, R. Jedicke^b, A. Fitzsimmons^c, L. Denneau^b, M. Granvik^{d,e}, B. Bolin^{b,f}, S. Chastel^b, R. J. Wainscoat^b, W. S. Burgett^g, K. C. Chambers^b, H. Flewelling^b, N. Kaiser^b, E. A. Magnier^b, J. S. Morgan^b, Paul A. Price^b, J. L. Tonry^b, C. Waters^b

^aFaculty of Mathematics, Physics and Informatics, Comenius University in Bratislava, Mlynská Dolina F1, 84248 Bratislava, Slovakia

^bInstitute for Astronomy, University of Hawaii at Manoa, 2680 Woodlawn Drive, Honolulu, HI 96822, USA

^cQueen's University Belfast, Belfast BT7 1NN, Northern Ireland, UK

^dDepartment of Physics, P.O. Box 64, 00014 University of Helsinki, Finland

^eFinnish Geospatial Research Institute, P.O. Box 15, 02430 Masala, Finland

^fUNS-CNRS-Observatoire de la Côte d'Azur, BP 4229, 06304 Nice Cedex 4, France

^gGMTO Corp., 251 S. Lake Ave., Suite 300, Pasadena, CA 91101, USA

Abstract

We present the results of a Monte Carlo technique to calculate the absolute magnitudes (H) and slope parameters (G) of $\sim 240,000$ asteroids observed by the Pan-STARRS1 telescope during the first 15 months of its 3-year all-sky survey mission. The system's exquisite photometry with photometric errors ≤ 0.04 mags, and well-defined filter and photometric system, allowed us to derive accurate H and G even with a limited number of observations and restricted range in phase angles. Our Monte Carlo method simulates each asteroid's rotation period, amplitude and color to derive the most-likely H and G , but its major advantage is in estimating realistic statistical+systematic uncertainties and errors on each parameter. The method was confirmed by comparison with the well-established and accurate results for about 500 asteroids provided by Pravec et al. (2012) and then applied to determining H and G for the Pan-STARRS1 asteroids using both the Muinonen et al. (2010) and Bowell et al. (1989) phase functions.

Keywords: Solar system, Near-Earth objects, Asteroids, Data Reduction Techniques

1. Introduction

Asteroid diameters are critical to understanding their dynamical and morphological evolution, potential as spacecraft targets, impact threat, and much more, yet most asteroid diameters are uncertain by $> 50\%$ because of the difficulties involved in calculating diameter from apparent brightness. The problem is that an

Email address: veres@fmph.uniba.sk (P. Vereš)

asteroid’s apparent brightness is a complicated function of the observing geometry, their irregular shapes, rotation phase, albedo, lack of atmosphere, and their rough, regolith-covered surfaces. Most of these data are unknown for most asteroids. The issue has been further confused because catalogued apparent magnitudes for individual asteroids may have been reported by numerous observers and observatories over many years (even decades) in a variety of photometric systems with varying concern for ensuring accuracy and precision. This work describes our process for calculating asteroid absolute magnitudes (from which diameter is calculated) and their statistical and systematic uncertainties for hundreds of thousands of asteroids using sparse but accurate and precise data from a single observatory, the Pan-STARRS1 facility on Maui, HI, USA. Our technique is suited to estimating absolute magnitudes when the phase curve coverage is even more sparse than those obtained by the Palomar Transient Factory (Law et al., 2009).

An asteroid’s absolute magnitude, H , is the apparent Johnson V-band magnitude, m , it would have if observed from the Sun at a distance of 1 au (i.e. observed at zero phase angle and 1 au distance). Accurate measurements of H as a function of time, together with infrared, polarimetric and radiometric observations, can provide crucial information about an asteroid’s size and shape, geometric albedo, surface properties and spin characteristics.

In 1985 the International Astronomical Union (IAU) adopted the two-parameter phase function developed by Bowell et al. (1989, hereafter B89), $\Phi_B(\alpha; H_B, G_B)$, describing the behavior of the apparent magnitude:

$$m(r, \Delta; H_B, G_B) = 5 \log(r\Delta) + \Phi_B(\alpha; H_B, G_B) \quad (1)$$

where Δ represents the topocentric distance, r the heliocentric distance, and $\alpha(r, \Delta)$ is the phase angle, the angle between the Earth and Sun as observed from the asteroid. We denote absolute magnitude in the B89 system as H_B with a corresponding slope parameter, G_B , that depends in a non-analytical manner on (at least) an asteroid’s albedo and spectral type (B89; Lagerkvist and Magnusson, 1990). The slope parameter determines how strongly the apparent brightness of an asteroid depends on the phase angle and accounts for the properties of scattered light on the asteroid’s surfaces. G_B has an average value of ~ 0.15 (B89) for the most numerous S and C-class main belt asteroid taxonomies. An accurate determination of both H_B and G_B requires a wide and dense time coverage of the object’s apparent magnitude. Therefore, it is not surprising that only a few tens of slope parameters were measured before the advent of dedicated CCD asteroid surveys.

The B89 phase function was very successful, but observations in the past twenty years have shown it can not reproduce the opposition brightening of E-type asteroids, the linear phase curve of the F-type asteroids,

and fails to accurately predict the apparent brightness of asteroids at small phase angles. To address these issues Muinonen et al. (2010, hereafter M10) introduced an alternative phase function, ϕ_M , with two slope parameters, G_1 and G_2 that uses cubic splines to more accurately describe the behavior of the apparent magnitude. An alternative M10 formulation with a single slope parameter, G_{12} that is denoted in our work as G_M , can be used when the data are not sufficient to derive the values of the two-parameter formulation i.e. $m = 5 \log(r\Delta) + \Phi_M(\alpha; H_M, G_M)$. Their phase function was constructed such that $H_M \sim H_B$ and the average asteroid would have a slope parameter of $G_M \sim 0.5$. This form of the phase function can provide better apparent magnitude predictions but derivation of H_M and G_M still requires extensive light curve coverage and well-calibrated observational data (Oszkiewicz et al., 2012). The IAU adopted the M10 (H, G_1, G_2) system as the new photometric system for asteroids in 2012.

In the remainder of this work we use H and G to represent ‘generic’ absolute magnitudes and slope parameters respectively, and use the subscripts B and M on each parameter when referring to the values calculated using the B89 and M10 phase functions respectively. We implemented both functions to facilitate comparison with 1) past work that used the B89 parameterization and 2) future work that will use the now-standard M10 implementation. When we use G_M we specifically mean the M10 G_{12} parameter.

The accuracy of most reported absolute magnitudes is poor due to the lack of good photometry and limited phase curve coverage. Jurić et al. (e.g. 2002) first reported a systematic error of about 0.4 mags in the MPC’s absolute magnitudes which the MPC (and others) now attempt to address with observatory-dependent corrections to the reported apparent magnitudes.

The determination of G has traditionally been even more of a challenge — they are so difficult to measure that they have only been calculated for $\ll 0.1\%$ of asteroids and, even then, the uncertainty is usually large (Pravec et al., 2012). An accurate measurement requires dense coverage of the phase curve and observations at different viewing aspects on the asteroid i.e. sub-solar positions. The vast majority of asteroids have no measured slope parameter so the average values of $G_B = 0.15$ or $G_M = 0.5$ are used. This assumption translates into a systematic error in an individual asteroid’s H and G , and large uncertainty on the distribution of the parameters in the population. The problem is particularly acute for objects that have been observed only at large phase angles e.g. resonant objects like 3753 Cruithne (de la Fuente Marcos and de la Fuente Marcos, 2013; Wiegert et al., 1997), and objects that orbit the Sun entirely within Earth’s orbit (Zavodny et al., 2008) for which absolute magnitudes might be in error by up to about 1 mags.

In summary, the problems with our current knowledge of asteroid absolute magnitudes and slope parameters are due to:

1. Reporting observations to the Minor Planet Center (MPC) in non-standard filters and/or without accurate calibration.
2. Not performing the color transformation from the filter used for an observation to the Johnson V-band for an asteroid's (usually unknown) color.
3. The lack of information about the photometric uncertainty on each observation reported to the MPC so that it must be statistically 'back-calculated' for each observatory (or observer) from historical observations.
4. The MPC database storing photometric values with only 0.1 mags precision.
5. Assuming that $G_B = 0.15$ for all asteroids that do not have a reported value for the slope parameter.
6. The accepted 'standard' average slope parameter of $G_B = 0.15$ for S and C class asteroids being different from the actual value of $G_B = 0.20$ (Pravec et al., 2012).
7. Sparse observations (in time). The lack of information about their rotation amplitudes induces an error and uncertainty in H .
8. Selection effects (Jedicke et al., 2002) that bias the discovery of asteroids towards their rotation amplitude maxima which induce a systematic error in their derived H .
9. Most of the effort in deriving H and G focuses on their statistical uncertainties when the systematic uncertainties dominate.

In this work we address each of these issues and derive the (H_B, G_B) and (H_M, G_M) parameters for known asteroids in the inner solar system out to, and including, Jupiter's Trojan asteroids. All the data were acquired by a single wide-field survey, Pan-STARRS1 (Kaiser et al., 2010), in standard filters with measured transformations to an accepted photometric system yielding photometric uncertainties that are typically about an order of magnitude smaller than earlier surveys. We use a Monte Carlo technique to measure the systematic errors introduced by filter transformations for unknown spectral types, unknown G , and the unknown asteroid spin and amplitude.

2. Pan-STARRS1 asteroids.

The Panoramic Survey Telescope and Rapid Response System's prototype telescope (Pan-STARRS1; Kaiser et al., 2010) was operated by the PS1 Science Consortium during the time period in which the data used in this study was acquired. The telescope has a 1.4 gigapixel camera (Tonry and Onaka, 2009) and 1.8 meter f/4 Ritchey-Chretien optical assembly and has been surveying the sky since the second half of

2011. Although the scientific scope of the survey is wide — including the solar system, exoplanets, brown dwarfs, stellar astronomy, galaxies, cosmology, etc. — most of the data products are suitable for asteroid science. About 5% of the survey time was dedicated to the ‘Solar System’ (SS) survey (more accurately a survey for near-Earth objects, NEO) through the end of 2012, was increased to about 11% from then till 2014 March 31, and the system is now 100% dedicated to NEO surveying.

Pan-STARRS1 surveys in six broadband filters, four of which were designed to be similar to the Sloan Digital Sky Survey photometric system (SDSS; Fukugita et al., 1996). Most of the observing time was devoted to the 3π survey of the sky north of -30 arcdeg declination for which each field was observed up to $20\times$ /year in each of 5 filters — g_{P1} , r_{P1} , i_{P1} , z_{P1} and y_{P1} . In the 3π survey the same field is observed 2 or 4 times on a single night in 30-40 second exposures obtained within about an hour. The dedicated solar system survey used only the wide-band w_{P1} filter that is roughly equivalent to $g_{P1} + r_{P1} + i_{P1}$ with 45 second exposures and a cadence of ~ 20 min to image the same field $4\times$ /night. The SS survey typically included fields within about 30 arcdeg of opposition or at small solar elongations ranging from 60 arcdeg to 90 arcdeg of the Sun.

Image processing was performed automatically and almost in real time by the Image Processing Pipeline (IPP; Magnier, 2006). Transient objects were identified after ‘difference imaging’ (Lupton, 2007) in which two consecutive images were convolved and subtracted to identify moving, or stationary but variable, targets. The photometric calibration until May 2012 was based on combined fluxes of bright stars from Tycho, USNO-B and 2MASS catalogs. Since that time the entire northern sky has been imaged by Pan-STARRS1 in all 5 filters allowing the development and use of the Pan-STARRS1 star catalog with ‘ubercalibrated’ magnitudes and zero points providing photometric uncertainties of $\sim 1\%$ (Schlafly et al., 2012; Magnier et al., 2013).

Moving transient detections are identified and linked into tracklets by the Moving Object Processing System (MOPS; Denneau et al., 2013) and tracklets are associated with known asteroids by known server (Milani et al., 2008). As of May 2015 the Pan-STARRS1 MOPS team has submitted $\sim 16,700,000$ positions and magnitudes of 575,000 known asteroids to the MPC representing 85% of all numbered asteroids. During the same time period the system discovered $\sim 41,000$ asteroids, among them about 850 NEOs and 46 comets, and reported about 2,500,000 detections of unknown asteroids to the MPC. About $\sim 42\%$ of the detections were in the w_{P1} filter acquired during the solar system survey while only about 9% were in the y_{P1} and z_{P1} bands.

To ensure a consistent data set of high quality photometry (Fig. 1) we restricted the detections used in

this study to known asteroids in the inner solar system (out to and including Jupiter’s Trojans) with multi-opposition orbits acquired during a sub-set of the 3π and solar system surveys between February 2011 and May 2012 (see Table 1) The detections were selected from the IPP’s calibrated chip-stage PSF-fit photometry (Schlafly et al., 2012) and were required to be unsaturated, with $sn > 5$, and not blended with stars or image artifacts. The Pan-STARRS1 IPP never implemented the capability of fitting trailed asteroid detections, so we restricted our data sample to asteroids that trailed by less than 5 pixels during the exposure, equivalent to the typical PSF-width of $\sim 1 \text{ arcsec}$. This limited the maximum rate of motion of the asteroids to about 0.75 deg/day , excluding most NEOs and even fast-moving asteroids like Hungarias and Phocaeas on the inner edge of the main belt. Our strict criteria resulted in a set of more than one million detections of approximately 240,000 asteroids

Table 1: Percentage of Pan-STARRS1 asteroid detections in each filter in the time period from February 2011 to May 2012 (values do not add to 100% due to rounding).

Band	g_{P1}	r_{P1}	i_{P1}	y_{P1}	z_{P1}	w_{P1}
Fraction (%)	18	20	17	2.2	6.2	36

Despite the enormous number of asteroid detections there are only about 10 detections/asteroid and each object is observed on average on only ~ 3 different nights over a phase angle range spanning about 7 arcdeg (Fig. 1). Therefore, the survey pattern does not typically allow the determination of an asteroid’s spectral type, rotation amplitude or period. The detections have a mean \pm RMS photometric uncertainty of $0.04 \pm 0.02 \text{ mags}$ and average \pm RMS visual magnitude of $19.8 \pm 1.2 \text{ mags}$. The photometric uncertainty mode is $\sim 0.02 \text{ mags}$ corresponding to $sm \sim 50$ detections. This surprisingly high value is due to our selection criteria: the multi-opposition objects were identified in earlier surveys with smaller telescopes so they are typically brighter when observed with Pan-STARRS1. Note that only $\sim 1\%$ of the detections in our data sub-set have a photometric uncertainty greater than the 0.1 mags precision provided by the MPC.

3. Method

This work introduces a Monte Carlo technique to determine H (and G when possible) and its statistical+systematic uncertainty based on the generation of synthetic asteroids (clones) that are each consistent

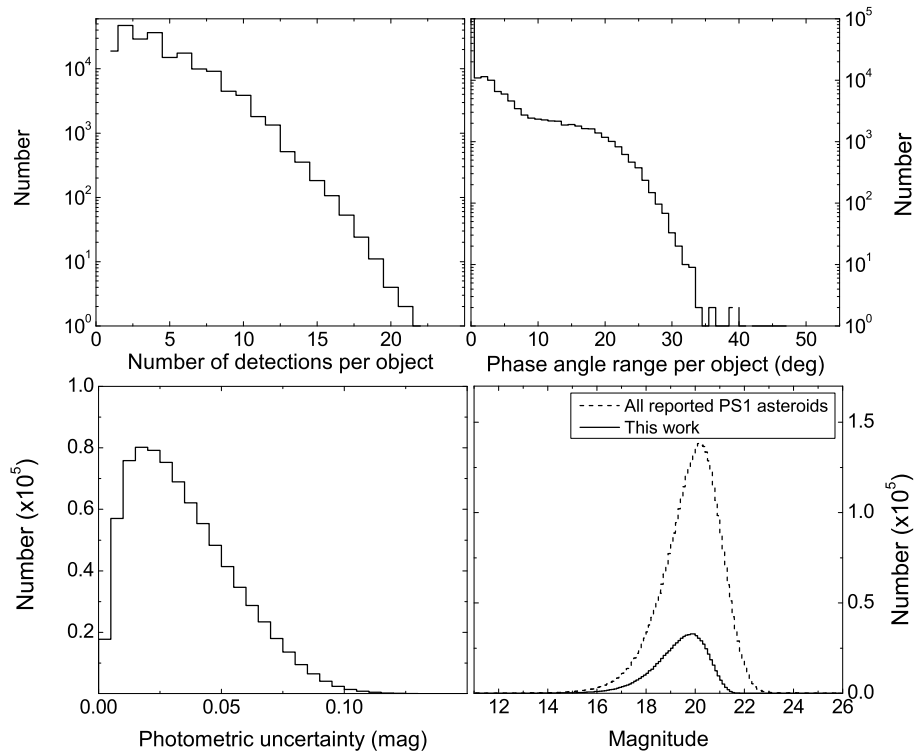


Figure 1: Characteristics of PS1 asteroid detections used in this work. (clockwise from top left) number of detections per object, phase angle range per object, apparent V-magnitudes, and photometric uncertainties per detection.

with the known asteroid. The clones explore the phase space of light curve rotation amplitudes, periods, colors and slope parameter in an attempt to replicate the observed apparent magnitudes. Each clone's observations are evaluated individually in the fitting process to derive H and G in the same manner as the actual observations so that the distribution of values for each object's clones provide a measure of the systematic errors in the values.

3.1. Step 1: Initial fit for H and G

The first step is essentially identical to the typical technique for calculating H and G : we fit the apparent V-band magnitude to the B89 and M10 phase functions using the IDL procedure `mpfit2dfun`¹ that employs the Levenberg-Marquardt least-squares fitting technique (Levenberg, 1944; Marquardt, 1963) to minimize the variance between the detections’ apparent magnitudes and the values predicted by the models. We converted the Pan-STARRS1 apparent magnitudes to V-band using taxonomy-dependent filter transformations if the asteroid’s taxonomy was specified by Hasselmann et al. (2012) and, if not, the mean S+C class color (see Table 2).

Table 2: Asteroid magnitude transformations from Pan-STARRS1 AB filter magnitudes to the Johnson-Cousin V- system based on Tonry et al. (2012). Solar colors are also included for reference.

Taxonomy	V-g _{P1}	V-r _{P1}	V-i _{P1}	V-z _{P1}	V-y _{P1}	V-w _{P1}
Sun	-0.217	0.183	0.293	0.311	0.311	0.114
Q	-0.312	0.252	0.379	0.238	0.158	0.156
S	-0.325	0.275	0.470	0.416	0.411	0.199
C	-0.238	0.194	0.308	0.320	0.316	0.120
D	-0.281	0.246	0.460	0.551	0.627	0.191
X	-0.247	0.207	0.367	0.419	0.450	0.146
Mean (S+C)	-0.28	0.23	0.39	0.37	0.36	0.16

The initial fits also use the mean class-dependent G provided in Table 3 if the taxonomic class is specified in the SDSS database (Hasselmann et al., 2012) but, if the class is not known, we use the mean of the S- and C-class values: $\overline{G}_B = 0.15$ (B89) and $\overline{G}_M = 0.53$ (Oszkiewicz et al., 2012) respectively.

The initial fits provided the absolute magnitudes in both photometric systems, $H_{B,i}$ and $H_{M,i}$, that were the inputs to the next step in the pipeline.

3.2. Step 2: Generating asteroid clones

Our final H and G estimates are the result of Monte Carlo (MC) simulations that require the generation of synthetic ‘clones’ for each of the asteroids in our sample. Each of the clones is generated with its own

¹ Markwardt IDL library, <http://www.physics.wisc.edu/~craigm/idl>

Table 3: Average slope parameters, G_B and $G_M \equiv G_{12}$, adopted in this work for 5 asteroid taxonomic classes as measured by Pravec et al. (2012) and Oszkiewicz et al. (2012) respectively. The 6th row provides ‘standard’ averages for the dominant S and C taxonomies.

Taxonomic Class	$G \equiv G_B$ $\pm(\text{RMS})$	$G_{12} \equiv G_M$ $\pm(\text{RMS})$
Q	0.25 ± 0.13	0.41 ± 0.14
S	0.24 ± 0.06	0.41 ± 0.16
C	0.15 ± 0.09	0.64 ± 0.16
D	0.09 ± 0.09	0.47 ± 0.14
X	0.20 ± 0.09	0.48 ± 0.19
S+C	0.15	0.53

color, slope parameter, rotation period, light curve amplitude and phase, where each of the parameters is selected from a unbiased distribution as described below.

3.2.1. Clone colors

Our pipeline can assign each clone the color of its parent asteroid (if known) or, when the parent’s color is not known, a random color based on an appropriate mix of taxonomies as a function of semi-major axis. About 16% of the asteroids in our sample have taxonomies defined by Hasselmann et al. (2012) (SDSS).

We implemented this technique by dividing the inner solar system into 4 zones (see table 4): NEO-like ($a < 2 au$), main belt ($2 au \leq a < 3.7 au$), Hildas ($3.7 au \leq a < 4.5 au$) and Trojans ($4.5 au \leq a < 6.0 au$). The semi-major limits defining the zone edges were set at or near a minimum in the number distribution as a function of semi-major axis and by the availability of published taxonomic distributions. The exact values make little difference to this work. We used the published, debiased taxonomic distributions in Table 4 in the 4 zones with the qualification that for the main belt (Mothé-Diniz et al., 2003) we aggregated many related taxonomic types into 3 broad spectral classes: S-class=(A, AQ, AV, O, OV, S, SA, SO, SQ, SV, V, L, LA, LQ, LS), X-class=(X, XD, XL, XS), and Q-class=(Q, QO, QV). We required that the fraction, $f(c, z)$, of asteroids with spectral class c in zone z satisfies $\sum_c f(c, z) = 1$. In the main belt, zone 2, we were able to generate the taxonomies as a finer function of a as provided by (Mothé-Diniz et al., 2003) with a similar

requirement that $\sum_c f(c, a) = 1$ at each semi-major axis.

Table 4: Taxonomic distribution of asteroids in 4 semi-major axes zones used in this work. The main belt values are given below at a representative $a = 2.5 au$ but we generated the clone taxonomies as a smooth function of semi-major axis in the range $2.0 au \leq a < 3.2 au$ as specified by Mothé-Diniz et al. (2003).

Taxonomy	zone 1	zone 2	zone 3	zone 4
	NEO-like ^a	MB ^b	Hilda ^c	Trojans ^d
	$a < 2 au$	$a \sim 2.5 au$	$3.7 au \leq a < 4.5 au$	$4.5 au \leq a < 6 au$
Q	14	0	0	0
S	23	61	0	0
C	10	30	7	10
D	18	0	67	80
X	35	9	26	10

^a Stuart and Binzel (2004)

^b Mothé-Diniz et al. (2003)

^c Grav et al. (2012)

^d Grav et al. (2012)

3.2.2. Clone slope parameters

We assigned slope parameters to the clones as a function of their assigned taxonomic class (c). i.e. the k^{th} clone was assigned a slope parameter $G_k(c) = \text{ran}[\overline{G}(c), \sigma_G(c)]$ where $\text{ran}[x, y]$ is a random number generated from a normal distribution with mean x and standard deviation y , and $\overline{G}(c)$ and $\sigma_G(T)$ are the mean and RMS of the distribution of slope parameters for class c , respectively (Table 3).

3.2.3. Clone rotation periods, amplitudes and phases

The sparse Pan-STARRS1 data did not allow us to measure any asteroid's rotation period and light curve amplitude. Furthermore, $< 2\%$ of the asteroids in our sample have measured light curves reported in the asteroid light curve database (LCDB²; Warner et al., 2009; Waszczak et al., 2015) The lack of this

² The asteroid lightcurve database is publicly available at <http://www.minorplanet.info/lightcurvedatabase.html>

information introduces systematic uncertainty and error into the absolute magnitude and slope parameter determination. We quantified these effects using our Monte Carlo technique with synthetic sinusoidal light curves for each clone.

Asteroid brightness variations on the hours-to-days timescales are usually caused by their non-spherical shape and rotation (the exceptions are for the unusual cases where the phase angle changes rapidly for close approaching NEOs, for multiple-systems in which brightness changes can occur if the objects transit or eclipse each other, and for objects with significant color variations). We assumed that the observing geometry (i.e. phase angle) effect on the asteroids' light curves are negligible in the Pan-STARRS1 data because of the limited range in phase angle coverage in our sample (Fig. 1). For the purpose of generating the clones' light curves we assumed that all the objects are triaxial ellipsoids that generate simple sinusoidal light curves with peak-to-peak amplitude A , period P , and rotation phase θ . The offset from the unmodulated light curve at time t is then $\Delta m(t) = A \sin(2\pi t/P + \theta)/2$.

Light curve amplitudes tend to be larger for smaller asteroids (see Fig. 2, Warner et al., 2009), probably because the smaller objects tend to be more irregularly shaped. Overall, the set of measured amplitudes and periods will be larger and shorter respectively than the true distribution because of observational selection effects, larger amplitudes and shorter periods are easier to detect and measure.

To reduce the impact of the light curve amplitude and period selection effects we employed the debiased distributions derived by Masiero et al. (2009) that are representative of asteroids with $H \sim 18$ (the average \pm RMS absolute magnitude in their study was 17.7 ± 1.4 mags). i.e. for objects with $H \sim 18$ they provide the cumulative fraction of asteroids, $F_{amp,Mas}(A)$, with light curve amplitudes $< A$. We empirically estimate the cumulative distribution of light curve amplitudes at other absolute magnitudes $F_{amp}(A, H)$ by 'normalizing' to the median at $H = 18$ from the median at other values:

$$F_{amp}(A, H) = F_{amp,Mas} \left[A \times \frac{A_{med}(18)}{A_{med}(H)} \right] \quad (2)$$

where $A_{med}(H)$ is an empirical function (Fig. 2) representing the median amplitude of asteroids in the LCDB (Warner et al., 2009). Thus, given a clone's initial (§3.1) absolute magnitude, H_i , we generated a random light curve amplitude for the clone according to the cumulative fractional distribution given by eq. 2.

We followed a similar procedure in assigning each clone a rotation rate R or, equivalently, a rotation period $P \equiv 1/R$. Masiero et al. (2009) also provide the data from which we derive the cumulative fraction of asteroids, $F_{rot,Mas}(R)$, with rotation rates $< R$. Once again, their results are representative of asteroids with $H \sim 18$, about 2 mags fainter than the mean value in our data sample, so we developed an empirical

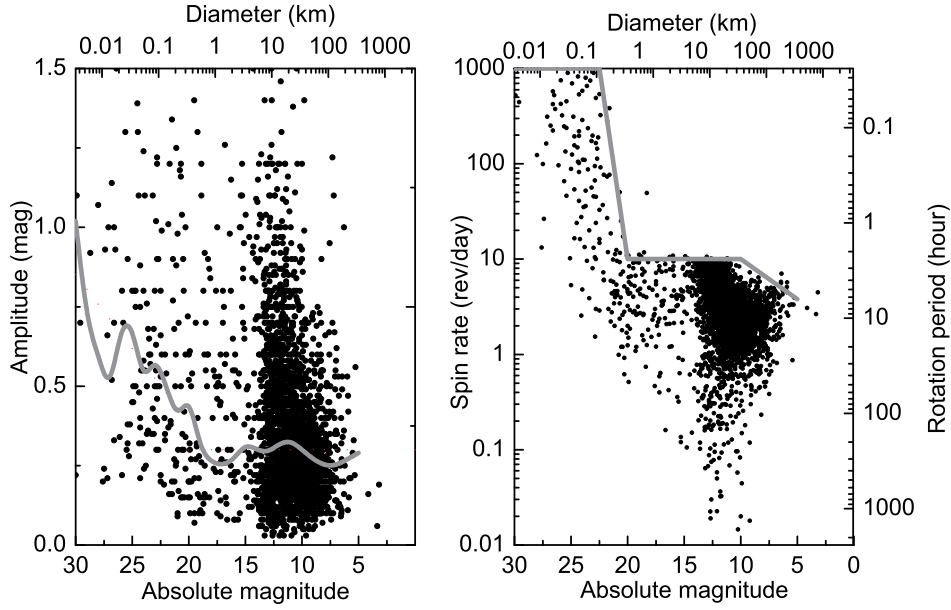


Figure 2: (left) Asteroid light curve amplitudes vs. absolute magnitude (H_B) from the LCDB (Warner et al., 2009). The solid gray curve represents the size-dependent moving median in 1.0 mags wide bins. (right) Measured asteroid spin rates (periods are provided on the right) vs. absolute magnitude (H_B) from the LCDB (Warner et al., 2009). The solid gray curve represents the size-dependent upper strength limit derived by Holsapple (2007).

technique to extend their cumulative fractional rotation rate distribution to other absolute magnitudes.

Asteroids with diameters > 100 meter ($H < 23$) have an empirically observed upper limit to their rotation rate of about 12 rev/day (Fig. 2) and about 99% of the distribution of debiased spin rates are < 12 rev/day (Masiero et al., 2009). Asteroids larger than a few tens of kilometers ($H < 12$) have an even more restricted upper limit to their rotation rates. We empirically defined an $R_{max}(H)$ as illustrated in fig. 2 and ‘compress’ or ‘expand’ the Masiero et al. (2009) distribution as necessary to create the cumulative fractional distribution at any H :

$$F_{rot}(R, H) = F_{rot, Mas} \left[R \times \frac{R_{max}(18)}{R_{max}(H)} \right]. \quad (3)$$

Once again, given a clone’s initial (§3.1) absolute magnitude, H_i , we generated a random rotation rate for the clone according to the cumulative fractional distribution given by eq. 3.

Finally, the rotational phase θ_k for the k^{th} clone was generated from a random uniform distribution in the range [0 arcdeg, 360 arcdeg).

Our light curves were simple sinusoids even though we understand that real asteroid light curves can be much more complicated. The technique could easily be extended to incorporate actual light curve properties or a more realistic distribution but i) only a tiny fraction of known asteroids have measured light curves ii) we will show below that our results are not particularly sensitive to the actual light curve parameter distribution and iii) if the actual light curve is known then there is no need for any of the methods developed here. i.e. this method only applies to the 98% of asteroids that do not have measured light curves. Since this is a preliminary work we have not made any effort to remove those asteroids that have published light curves.

3.3. Step 3: Refining H and G (First Monte Carlo simulation).

The first Monte Carlo (MC) simulation yields our MC estimate for H and G from the sparse Pan-STARRS1 phase curve coverage data. As described in detail above, we created 500 clones of each object where the k^{th} clone was assigned a taxonomic class (color) c_k , light curve amplitude A_k , and period P_k . We then fit for each clone's absolute magnitude, slope parameter and light curve phase, (H'_k, G'_k, θ'_k) , by minimizing the χ^2 with respect to the actual observations:

$$\chi_{k,obs}^2 = \sum_{j=1}^n \left[\frac{m_k(t_j; H'_k, G'_k, \theta'_k) - m(t_j)}{\delta m(t_j)} \right]^2 \quad (4)$$

where n is the number of observations (detections) of the object, $m(t_j)$ is the actual object's observed apparent magnitude, $\delta m(t_j)$ is the reported uncertainty on the actual Pan-STARRS1 apparent magnitude for that observation in the original filter, and m_k is the clone's predicted apparent magnitude at the actual time of observation, t_j , in the Pan-STARRS1 filter in which the observation was made, with the clone's appropriate color transformation ($\Delta m_k(t_j)$; Table 2):

$$m_k(t_j) = 5 \log[r(t_j)\Delta(t_j)] + \Phi[\alpha(t_j); H'_k, G'_k] + A_k \sin[2\pi t_j/P_k + \theta'_k]/2 + \Delta m_k(t_j), \quad (5)$$

and Φ is the B89 or M10 phase function.

The 'best' clone is the one (k^*) that produces the minimum χ^2 and we adopt that clone's H'_{k^*} and G'_{k^*} values as our MC estimate for the object's absolute magnitude and slope parameter. The process was run separately for both the B89 and M10 phase functions to provide our MC estimates for (H_B, G_B) and (H_M, G_M) respectively. To avoid unphysical values the fitting process required that $-0.25 \leq G_B \leq 0.8$ and $-0.5 \leq G_M \leq 1.5$.

We found that 500 clones provides a good balance between the computation time and our ability to estimate the uncertainty on the absolute magnitudes and slope parameters. It is likely that when there are only a small number of detections that the number of clones could be decreased but we did not pursue this simplification. When the number of detections becomes very large then our technique becomes unnecessary as either traditional (Pravec et al., 2012) or sparse light curve fitting (Muinonen et al., 2010; Law et al., 2009) becomes more effective.

3.4. Step 4: Estimating uncertainties and error on H and G (second Monte Carlo fit).

We estimated the uncertainties and errors on H'_{k^*} and G'_{k^*} by fitting for the absolute magnitude and slope parameter with purely synthetic light curves generated from the clone with the best fit. i.e. we re-applied the same method as described in Step 3 (§3.3) except that we fit the clones to the best synthetic object rather than the real object (we continue to use the sub-script k to refer to clones but the clones used here are distinct from the clones used in the last step):

$$\chi_{k^*,syn}^2 = \sum_{i=1}^n \left[\frac{m_k(t_j; H'_k, G'_k, \theta'_k) - m_{k^*}(t_j)}{\delta m_{k^*}(t_j)} \right]^2. \quad (6)$$

where $\delta m_{k^*}(t_j) = \delta m(t_j)$, i.e. the uncertainty on the synthetic observation at time t_j was set to the uncertainty on the actual observation at time t_j .

If we let X generically represent either H or G then the combined statistical+systematic uncertainty on X is the standard deviation of the clones' X distribution:

$$\delta X = \sqrt{\frac{1}{n} \sum_k (X'_k - \overline{X'})^2} \quad (7)$$

where $\overline{X'}$ is the average value of X for all the synthetic objects' clones. Similarly, the combined statistical+systematic error on X is the average error on the values for the synthetic clones:

$$\Delta X = \frac{1}{n} \sum_k (X'_k - X'_{k^*}) \quad (8)$$

3.5. Verification

We verified our method with two independent sets of synthetic data generated from real Pan-STARRS1 data: 1) 10,000 randomly selected known Pan-STARRS1 objects, most of them with sparse phase curve coverage and 2) the 1,000 known Pan-STARRS1 objects with the best phase coverage. To have better control over assessing our method's validity we generated photometric magnitudes and uncertainties with synthetic absolute magnitudes (H_B and H_M) and slope parameters (G_B and G_M) at each real time of observation with

the known object’s orbit. We then employed our pipeline to calculate each synthetic object’s H and G to measure the statistical and systematic errors induced by our technique. Moreover, we tested two different scenarios for assigning light curve amplitudes and periods to the clones: 1) the debiased distributions from Masiero et al. (2009), 2) and the observed distributions from the LCDB (Warner et al., 2009).

The result is that for both synthetic populations (sparse and dense phase curve coverage) and for both light curve amplitude-period relations (debiased and observed) the difference between the generated synthetic values and the values returned by our method was normally distributed with zero mean. i.e. our technique correctly derives the H and G . Use of the debiased or observed amplitude and period distributions does not affect the derived H and G at the level of photometric accuracy and uncertainty of the Pan-STARRS1 data with its associated phase curve coverage i.e. does not cause any systematic errors.

4. Results & Discussion

4.1. Absolute magnitudes comparison with Pravec et al. (2012)

We think Pravec et al. (2012)’s detailed light curve study of ~ 500 asteroids sets the standard in measuring asteroid photometric properties. They provided only H_B (it was before the adoption of the new IAU standard) but that value *should* be identical to H_M . Our results agree extremely well with Pravec et al. (2012) for the 347 objects that appear in both data sets (fig. 3). The mean differences of $H_B - H_{B,Prac} = -0.06 \pm 0.02$ mags and $H_M - H_{B,Prac} = 0.02 \pm 0.02$ mags are consistent with zero to within 3σ and 1σ respectively, with better agreement for the new IAU standard photometric system of M10. The RMS of each distribution is 0.36 mags and 0.29 mags respectively, due to the quadratic combination of the errors in both Pravec et al. (2012)’s and this work.

The distribution of $H_B - H_{B,Prac}$ is quasi-normally distributed (fig. 3) with an RMS of 0.31 mags including a tail extending to $H_B - H_{B,Prac} < -1$. Interestingly, the difference between our initial fits with assumed slope parameter (§3.1) and Pravec et al. (2012), $H_{B,i} - H_{B,Prac}$, is roughly normally distributed with a mean error of -0.06 ± 0.02 mags and RMS of 0.26 mags. Thus, the simple, traditional, fitting procedure with assumed G to our high-precision but sparse data produces comparable absolute magnitudes to the MC technique. The power of the MC technique lies in its ability to estimate the true statistical and systematic uncertainty in the absolute magnitude due to the unknown parameters in the analysis.

Our absolute magnitudes calculated with the M10 phase function (H_M) are better behaved (fig. 3) in the sense that the distribution is more normally distributed. The initial fit to the sparse data in the M10 system

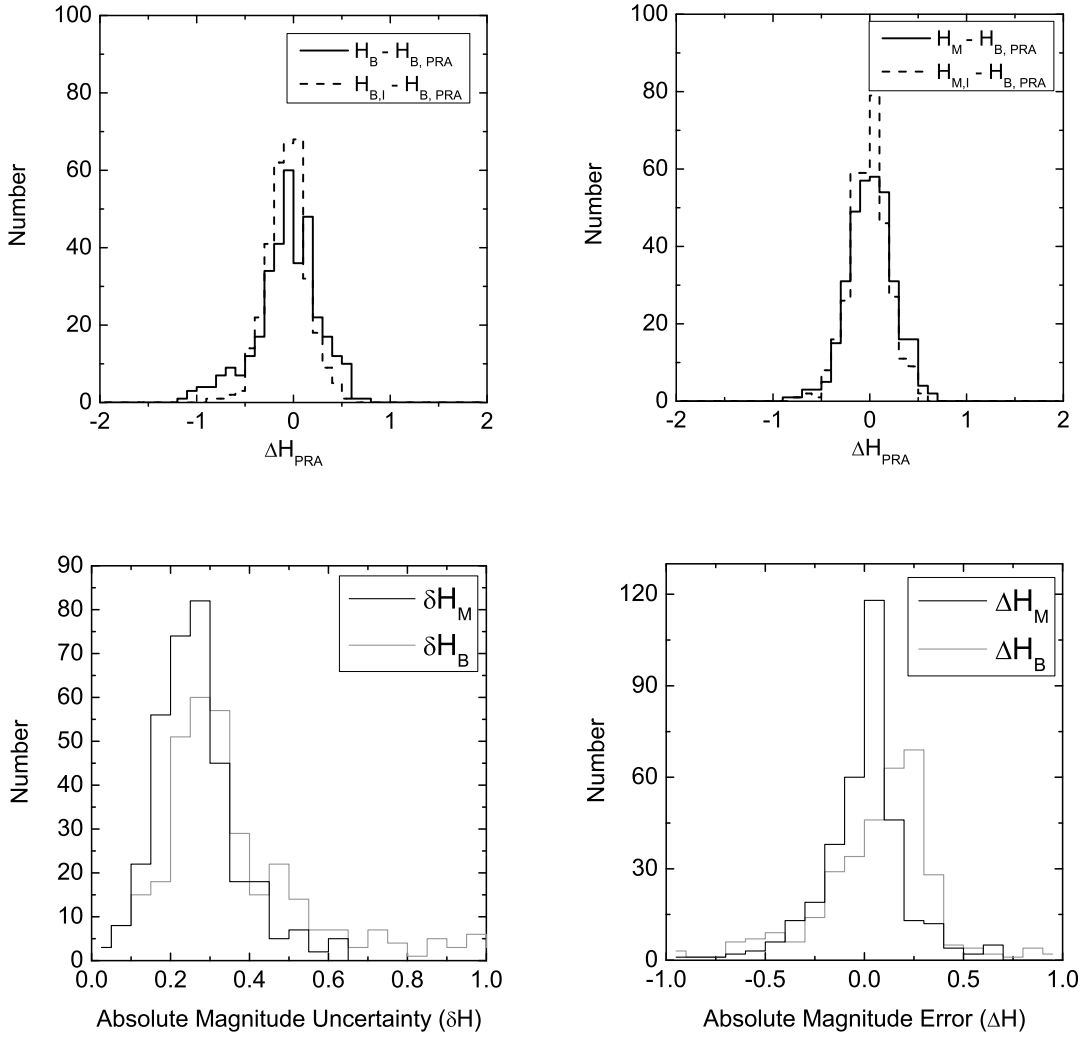


Figure 3: (top) Absolute magnitudes from our study compared with 347 objects in common with Pravec et al. (2012) using the B89 (left) and M10 (right) photometric systems. The dashed line shows the results of the traditional initial fit (§3.1) and the solid line provides the results of the MC fit (§3.3). (bottom-left) Uncertainties and (bottom-right) estimated systematic errors on absolute magnitudes from our study compared with those reported by Pravec et al. (2012).

provided absolute magnitudes with mean systematic errors of 0.00 ± 0.02 mags and $\sigma \sim 0.26$ mags compared to the MC technique with a mean error of 0.02 ± 0.02 mags and $\sigma \sim 0.28$ mags. The good behavior of both the MC and initial fits with M10 that results in a normal error distribution leads us to the conclusion that it

is superior for the determination of absolute magnitudes even for sparse data samples.

We also used the Pravec et al. (2012) values to test our technique (§3.4) for establishing the uncertainty and error on our measured absolute magnitudes. Their technique allows excellent control of all the statistical and systematic uncertainties in the H calculation because they observed targets for more than a decade in a systematically controlled program and had 2 to 3 orders of magnitude more data per object. Thus, they report H uncertainties about $3\times$ less than our uncertainties and we can compare our measured uncertainties (δH) to the RMS spread of $H - H_{Pra}$, and our measured error estimates to its average (fig. 3).

As stated earlier, the real power of the MC technique is its ability to estimate the statistical and systematic uncertainties on the derived H and G values. Our estimated absolute magnitude uncertainties (δH_B ; fig. 3; §3.4) for the asteroids that overlap the Pravec et al. (2012) data sample have the expected poissonian distribution with a mean of $\bar{\delta}_{H_B} = 0.36 \pm 0.01$ mags using the B89 phase function (fig. 3), comparable to the RMS of 0.37 ± 0.02 mags for the distribution of the error in our measurement, $H_B - H_{B,Pra}$, as expected. Similarly, our mean estimated systematic error of $\Delta H_B = 0.03 \pm 0.02$ mags agrees with the actual systematic offset in the $H_B - H_{B,Pra}$ distribution. We can compare our estimated uncertainties and systematic errors in the same manner for the M10 phase curve. Our estimated mean uncertainty, $\delta H_M = 0.26 \pm 0.01$ mags, is consistent with $RMS(H_M - H_{B,Pra}) = 0.28 \pm 0.02$ mags and our estimated systematic error of $\Delta H_M = 0.00 \pm 0.02$ mags, is consistent with $\overline{(H_M - H_{B,Pra})} = 0.02 \pm 0.02$ mags.

The good agreement between our results and those of Pravec et al. (2012) illustrates the utility of our MC technique at measuring an asteroid’s absolute magnitude and estimating the associated statistical+systematic uncertainty and any systematic bias, even for sparse data sets with limited phase angle coverage. Furthermore, the nice behavior of our results with the M10 phase curve and the good agreement between our H_M and $H_{B,Pra}$ provides evidence that $H_M \sim H_B$ when care is taken to ensure that the photometric data is of excellent quality.

4.2. Absolute magnitudes

Having established the utility of our technique on a well-controlled data set in the previous section we now employ it on all the asteroids in our selected Pan-STARRS1 data sample. We were able to calculate the absolute magnitudes with combined statistical and systematic uncertainties for more than 240,000 asteroids spanning the range from $6.4 < H < 26.5$ (fig. 4). The ~ 20 mags range corresponds to about a factor of 10,000 \times in the diameters of the objects and spans the inner solar system from the NEOs to Jupiter’s Trojan asteroids. Our sample represents $\sim 38\%$ of all known asteroids in that range as of February 2014, with the

highest completion of $\sim 75\%$ from $10.5 < H < 11.0$.

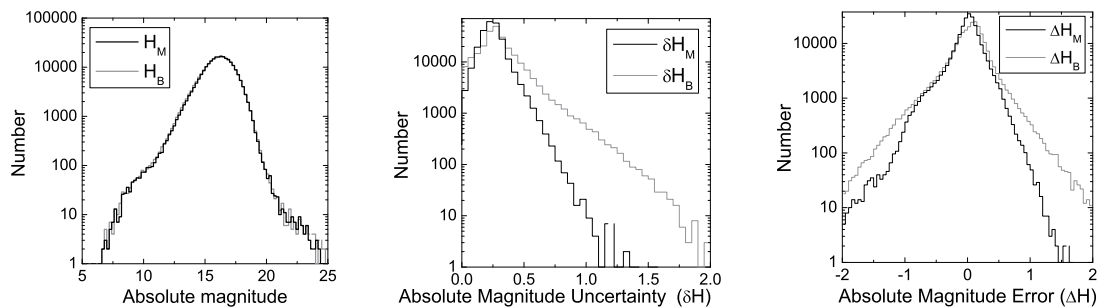


Figure 4: (left) Absolute magnitudes (H_M and H_B) of 248,457 asteroids. (center) Uncertainties and (right) estimated errors in the absolute magnitudes derived with our Monte Carlo method using the phase functions of (gray) B89 and (solid) M10.

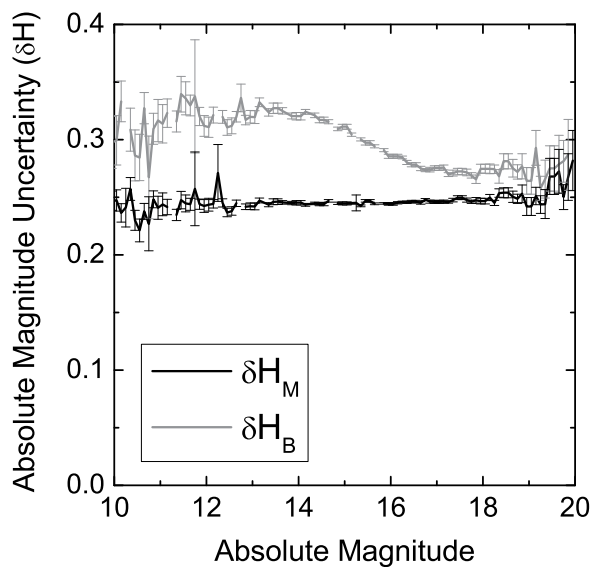


Figure 5: Absolute magnitude uncertainty as a function of H using the B89 (grey) and M10 (dark) methods.

The mean uncertainties of $\overline{\delta H_B} = 0.30 \pm 0.01$ mags and $\overline{\delta H_M} = 0.25 \pm 0.01$ mags (Fig 4) show that the new IAU photometric scheme of M10 is better than B89 for the sparse Pan-STARRS1 data and phase

coverage but this conclusion mis-represents the full utility of the M10 technique. For one, the M10 system uncertainty is almost uniform with $\delta H_M \sim 0.24$ mags for the entire range $10 < H < 20$ (fig. 5). Second, even though the two techniques yield approximately the same uncertainties for the faintest objects for which the uncertainty is dominated by the measurement statistics (fig. 5), the B89 method’s statistical uncertainty is $\sim 0.35\%$ larger for bright objects ($10 < H < 14$).

The mean of our estimated statistical+systematic error using the M10 method, $\overline{|\Delta H_M|} = 0.02 \pm 0.01$ mags, is comparable to the B89 method, $\overline{|\Delta H_B|} = 0.01 \pm 0.01$ mags (fig. 4). The error in the absolute magnitude for each asteroid is less than the estimated uncertainty in $\sim 62\%$ of all the asteroids in our H_B sample and $\sim 73\%$ in our H_M sample. The RMS of the $|\Delta H_B|$ and $|\Delta H_M|$ errors respectively of ~ 0.35 mags and ~ 0.25 mags confirms that the new IAU photometric system is an improvement over the earlier one and, furthermore, the shape of the error distribution is more reasonable for ΔH_M than ΔH_B (note the peak of ΔH_B is shifted by 0.05 mags from zero but the ΔH_M peak is near zero (fig. 4).

Overall, there is almost no difference between our M10 and B89 ensemble results for Pan-STARRS1 asteroids and the mean difference $\overline{H_M - H_B}$ is 0.03 ± 0.01 mags with RMS of 0.22 mags (fig. 6). The mean difference between the initial fit solutions is $\overline{H_{M,i} - H_{B,i}} = 0.05 \pm 0.01$ mags.

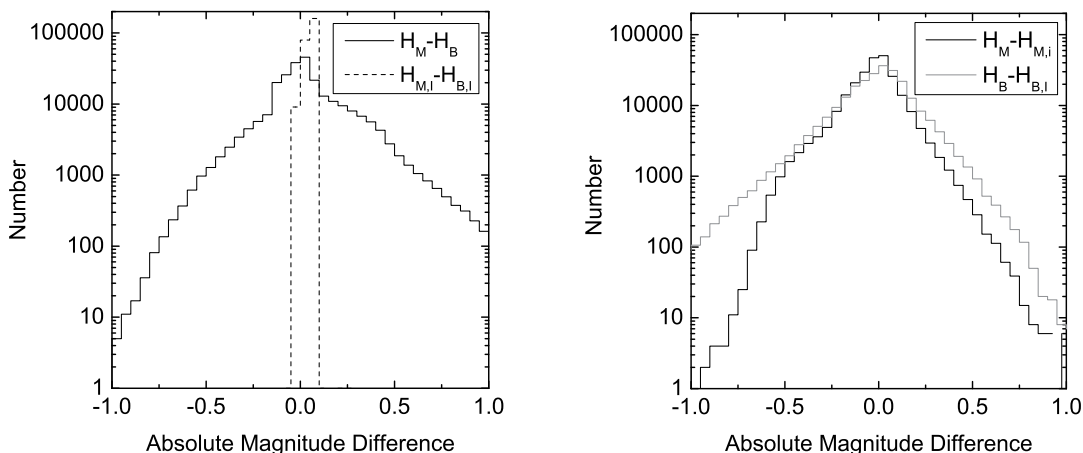


Figure 6: (left) Difference between the M10 and B89 absolute magnitudes for the MC and initial fit solutions. (right) Difference between MC and initial fit solutions for the absolute magnitude using the M10 and B89 methods.

On the other hand, the utility of restricting H and G analyses to data derived from well-calibrated single-

survey data is easily illustrated by comparing the results of our technique to the MPC database values that do their best to incorporate data from multiple telescopes and observers over many decades. The MPC currently only publishes absolute magnitudes using the B89 phase function and there is a mean difference of $\overline{H_M - H_{B,MPC}} = 0.26 \pm 0.01$ mags and $\overline{H_B - H_{B,MPC}} = 0.22 \pm 0.01$ mags between our technique and the MPC values. The consistency between the mean differences is at least reassuring and the RMS spread in values is due to 1) the systematics introduced by the MPC’s procedure that incorporates apparent magnitudes from many different observatories in many different passbands and 2) the systematics introduced by our sparse light curve coverage. Given that we established in §4.1 that our technique works well in comparison to the ‘standard’ Pravec et al. (2012) values, our conclusion is that the error is due to the MPC’s incorporation of photometry from different sites and filters over a long period of time. The error reported here is less than the ~ 0.4 mags value reported by Jurić et al. (2002), but since the time of that study the MPC database has been further populated by photometry from Pan-STARRS1 and other large surveys with better photometric calibrations than previous surveys. Hence, it is unsurprising that the $H_{B,MPC}$ values approach their correct values over time.

Our calculated uncertainties are about $2\times$ larger than reported by Oszkiewicz et al. (2012) who employed the entire MPC catalog for their input photometry and provided H_M and G_M for 421,496 asteroids — almost double our sample. For comparison with earlier works they also provided H_B and G_B . Their work was very difficult as it required calibrating and correcting the systematic problems intrinsic to the various observatories and observers that contributed the photometric data in multiple filters, but offered the advantage of an extensive data set with wide time and phase angle coverage i.e. much like the MPC technique described in the last paragraph. The systematic offset between our H_M values and Oszkiewicz et al. (2012) of $H_M - H_{M,Os} = 0.33 \pm 0.01$ mags (fig. 7) is similar to the offset derived between our results and the MPC.

Jurić et al. (2002) and Pravec et al. (2012) reported a systematic offset of about 0.38 mags to 0.5 mags between their calculated absolute magnitudes and the values reported by the MPC. Those values are in rough agreement with Waszczak et al. (2015) who reported H_B and G_B from over 54,000 asteroids observed in g and R -band with the Palomar Transient Factory (PTF). They measured a mean value of $R_{PTF} = V_{MPC} + 0.00$ which implies a systematic offset of ~ 0.4 mags in the MPC absolute magnitudes because the average $V - R$ for asteroids is ~ 0.4 . Our values (fig. 8) are consistent with the MPC for $H_B < 11$ mags and $H_B > 19$ mags, i.e. within < 0.1 mags of the MPC absolute magnitudes (their reported precision), but are systematically higher than the MPC absolute magnitudes for $11 \text{ mags} \ll H_B < 19 \text{ mags}$. i.e. our absolute magnitudes are systematically *fainter* than reported by the MPC and this would translate directly into predicting fainter

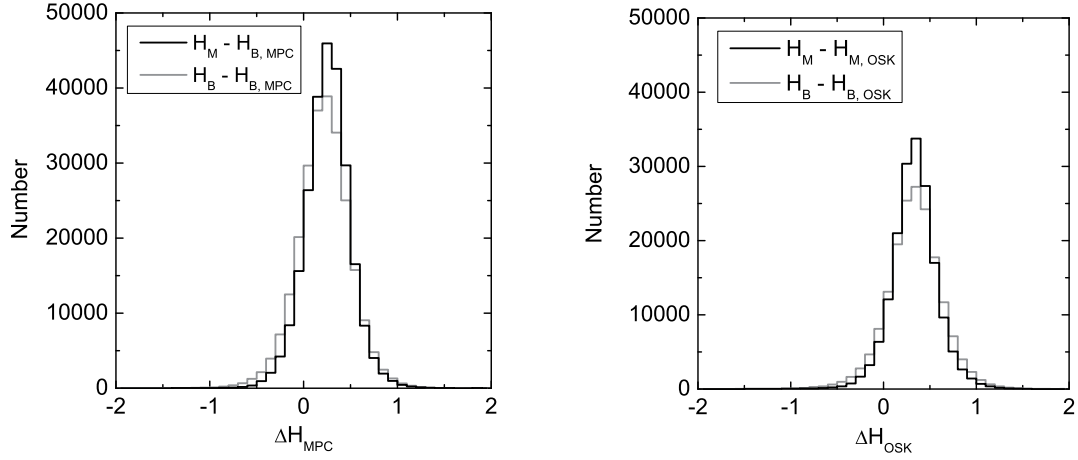


Figure 7: The difference between the H_B and H_M absolute magnitudes calculated in this work and (left) the Minor Planet Center and (right) Oszkiewicz et al. (2012). We compare our H_M to the MPC H_B because the two photometric systems should yield similar absolute magnitudes (in theory).

apparent magnitudes than the MPC and, similarly, suggesting that the objects are smaller than predicted by the use of the MPC absolute magnitudes. The systematic difference reaches a maximum of ~ 0.35 mags at $H_B \sim 14$ in agreement with the earlier studies. This magnitude offset has implications for developing observing programs, selecting objects for followup, and for studies of the asteroids' size-frequency distribution.

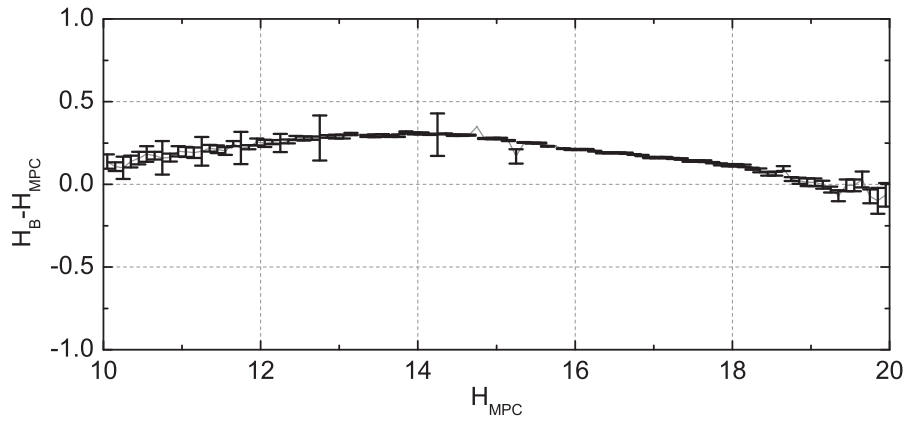


Figure 8: The difference between the absolute magnitude H_{MPC} reported by the MPC using the B89 phase function and this work's H_B value as a function of absolute magnitude (≤ 100 random data points are shown at each discrete H_{MPC} value in order to reduce confusion). The thick solid black line represents the average in each 0.1 mags wide bin and the standard error on the mean is shown with error bars. The error bars are about the width of the line for $13 < H_{MPC} < 18$.

4.3. Slope Parameters

The vast majority of Pan-STARRS1 asteroids offer only sparse phase angle coverage (Fig. 1) for the determination of the slope parameter but our MC technique should provide a realistic estimate of the statistical uncertainty and systematic error when the phase angle coverage is not too large and the detections are not in multiple apparitions.

The G_B distribution (fig. 9) is very wide with a peak near 0.15, the default slope parameter for objects of unknown spectral class (most of the asteroids in our sample). The distribution is artificially constrained between the lower and upper limits ($-0.25 < G_B < 0.8$). On the other hand, the G_M distribution has a broad peak centered on $G_M \sim 0.5$ superimposed on a roughly flat distribution of slope parameters between our artificial limits ($-0.5 < G_M < 1.5$). The large peak near $G_M = 0.2$ that contains $\sim 30\%$ of all G_M values is due to a discontinuity in the M10 phase function, it is not an error in our implementation. In comparison, $\sim 8\%$ of the Oszkiewicz et al. (2012) G_M values were also ~ 0.2 . Our technique is particularly sensitive to the function discontinuity and has a propensity to drive the fitted G_M value to 0.2 when the number of data points is small. We suggest that future attempts to use the M10 phase function flag and address this situation, perhaps by forcing $G_M = 0.5$ in those cases.

The slope parameter uncertainty (δG) distributions have peaks at zero corresponding to the $\sim 24\%$ of cases in both methods where the MC technique did not converge and we fixed the slopes. Those G_B that were actually fit have a normal-like distribution with mean $G_B = 0.18 \pm 0.01$ and RMS of 0.05 (Fig. 9). Similarly, the G_M uncertainty has a normal-like distribution with mean at 0.29 ± 0.01 and RMS of 0.17. The δG_M distribution is wider and shifted towards larger values than the δG_B distribution because the G_M values are fundamentally larger than the corresponding G_B values. The percentage uncertainties ($\delta G/|G|$, fig. 9) in both slope parameters are very similar, suggesting that the two phase functions are equally effective for calculating the slope parameters, at least in the regime applicable to this data sample. The mean relative slope parameter uncertainties are $\sim 34\%$ and $\sim 0.36\%$ for G_B and G_M respectively, the large values being due mostly to the limited phase curve coverage.

As expected, the slope parameter uncertainty depends on the phase angle coverage ($\Delta\alpha$, fig. 10). The uncertainty is artificially small at small phase angle ranges near zero because in these cases the slope parameter was mostly fixed at a pre-specified value. The uncertainty is largest for $\Delta\alpha \sim 5$ arcdeg because at this phase angle range the slope parameter begins to be calculable, and the uncertainty drops at larger phase-angle ranges because the data provides stronger constraints on the shape of the phase function. However, even in the best case scenario, for phase angle ranges of > 30 arcdeg, the percentage uncertainty is still $\sim 50\%$

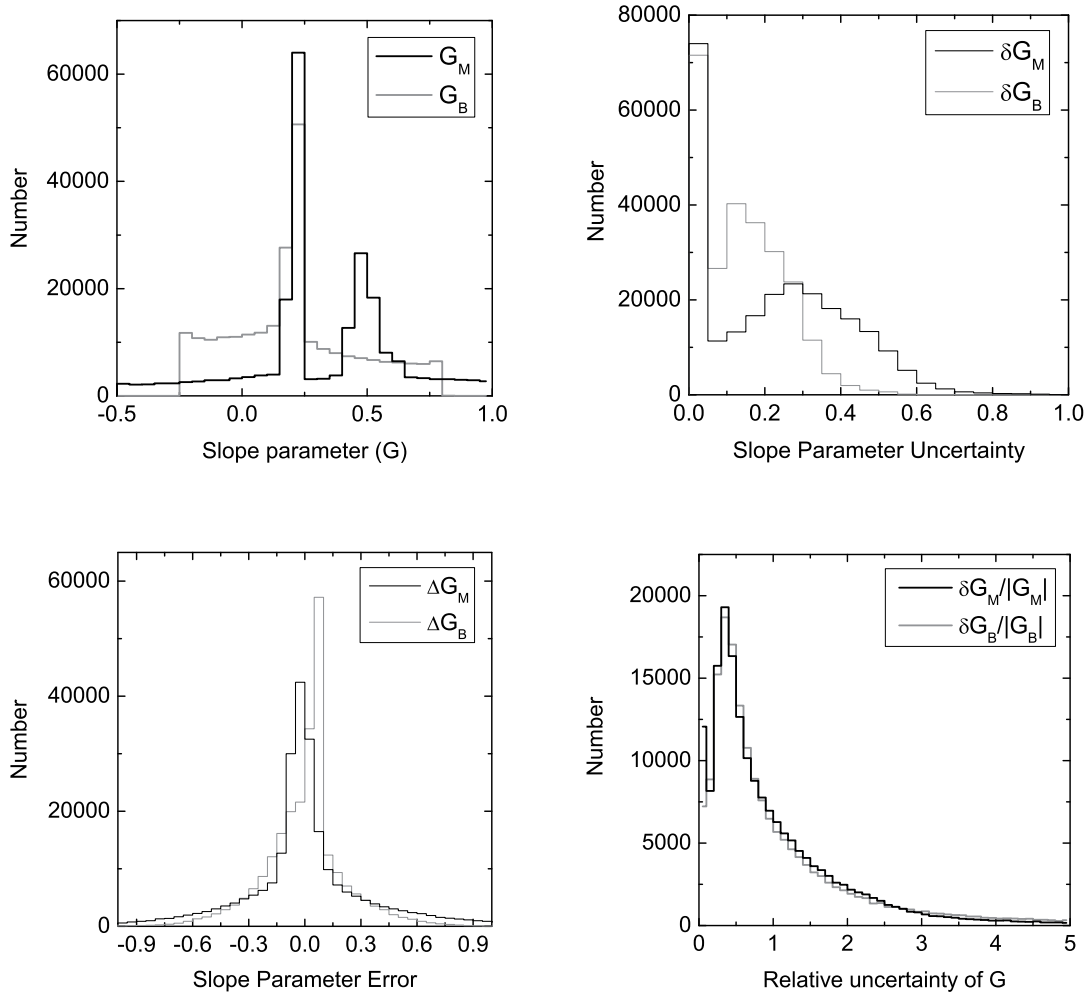


Figure 9: (top left) The slope parameters G_B (B89) and G_M (M10) and (top right) their uncertainties and (bottom left) errors. (bottom right) Percentage uncertainty in the slope parameter (δG) with the (gray) B89 and (black) M10 photometric methods.

for both phase functions. In any event, the number of objects in our data sample with large phase angle coverage is very small. Fig. 10 also illustrates that the systematic errors introduced by our MC technique are not dependent on phase angle coverage.

Pravec et al. (2012) provide accurate G_B slope parameters with uncertainties for more than 500 asteroids with densely covered light curves in a single pass band over a wide range of phase angles. The mean

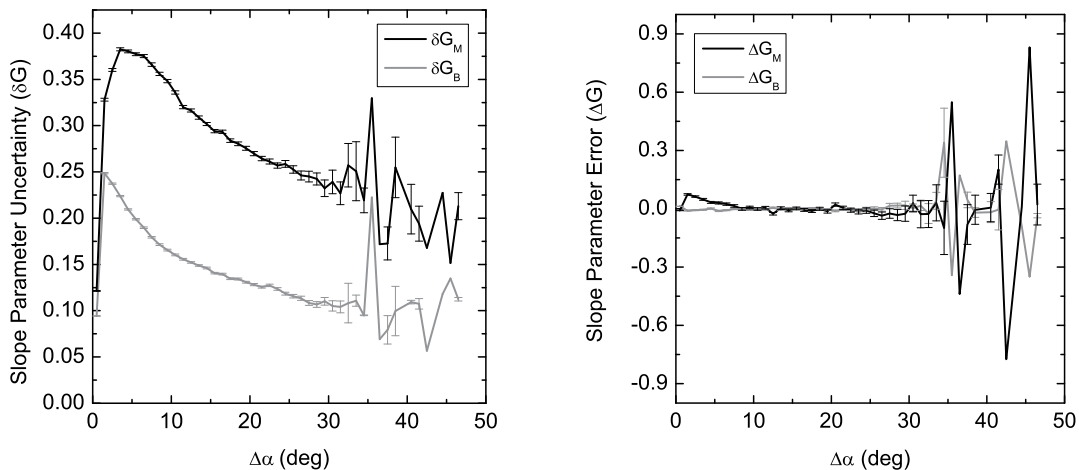


Figure 10: (left) Average MC slope parameter uncertainty and (right) error as a function of phase angle range using the (gray) B89 and (black) M10 phase functions.

difference between this work’s G_B and $G_{B,PRA}$ is 0.00 ± 0.02 with $\sigma \sim 0.28$ for the 196 asteroids in common between the two data sets with derived slope parameters (Fig. 11). The agreement between our MC solution and the accurate work of Pravec et al. (2012) using the B89 phase function suggests that our technique for calculating the slope parameter is viable for a large number of asteroids with sparsely sampled light curves. Furthermore, our technique allows us to estimate the mean error on the derived slope parameter, $\overline{\Delta G_B} = 0.00 \pm 0.01$, so the MC technique does not introduce a systematic bias. The mean statistical uncertainty in the slope parameter for our data sample of $\overline{\delta G_B} = 0.17 \pm 0.01$ is twice as large as the Pravec et al. (2012) data set of $\overline{\delta G_B} = 0.09 \pm 0.01$ which could be interpreted as either surprisingly good, given the small number of observations and phase curve coverage of our data sample, or as an indication that measuring G_B is difficult even with a very good data sample.

As described earlier, Oszkiewicz et al. (2012) derived asteroid slope parameters from photometry reported to the MPC from multiple observatories that used different filters and reference catalogs. They also had to deal with the fact that the MPC observation submission format did not allow reporting of photometric uncertainties. To reduce some of the associated problems they statistically calibrated the disparate datasets and used photometry only from major surveys. After excluding the artificial peak near $G_M = 0.2$ (i.e., excluding the range $0.18 < G_M < 0.22$), and including only those objects for which G was actually

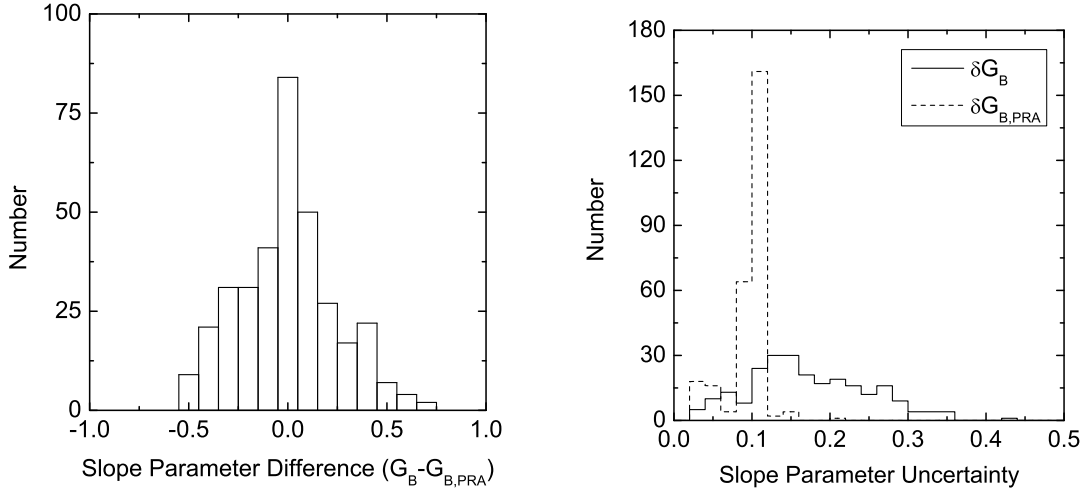


Figure 11: (left) The difference between our MC G_B values (B89) and 196 objects in common with Pravec et al. (2012). (right) Slope parameter uncertainty distributions for the same 196 objects for (solid) our MC values and (dashed) Pravec et al. (2012).

Table 5: Mean slope parameters \pm standard deviation (G_B , B89) derived in this work (PS1, second column) and by Pravec et al. (2012) (PRA12, third column) for the same objects in 4 major taxonomic classes. The last column is the number of common objects that have a Hasselmann et al. (2012) spectral classification (no D type asteroids satisfied our requirements on taxonomic identification and slope parameter determination).

Taxonomic Class	G_B PS1	G_B PRA12	N
Q	0.11±0.16	0.19 ± 0.10	3
S	0.16±0.26	0.23 ± 0.05	32
C	0.03±0.10	0.13 ± 0.01	4
D	n/a	n/a	0
X	0.21±0.30	0.20 ± 0.10	9

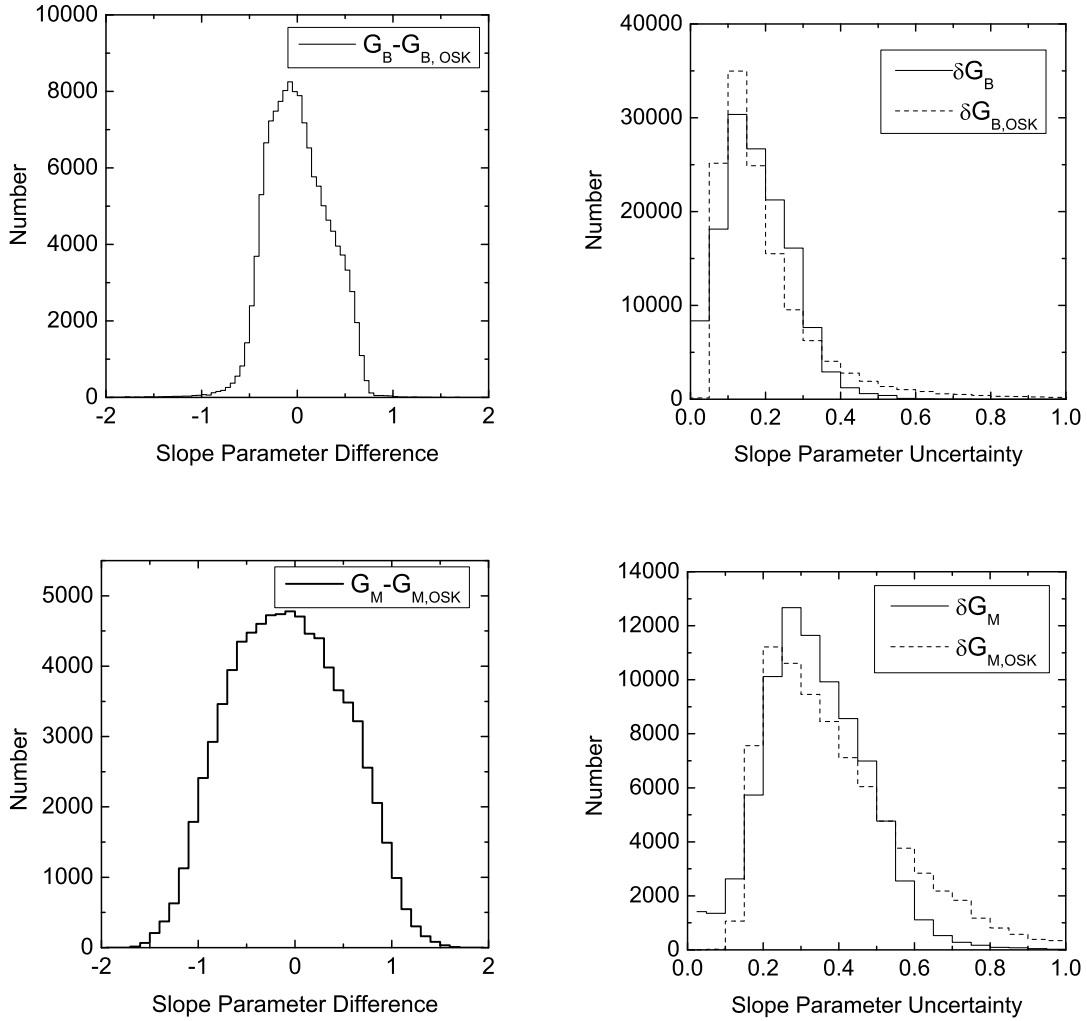


Figure 12: (top left) Difference between our MC G_B values (M10) and 133,885 objects in common with Oszkiewicz et al. (2012). (top right) Slope parameter uncertainties for the same objects as determined in this work and by Oszkiewicz et al. (2012). (bottom left) Difference between our MC G_M values (M10) and 80,756 objects in common with Oszkiewicz et al. (2012). (bottom right) Slope parameter uncertainties for the same objects as determined in this work and by Oszkiewicz et al. (2012).

fit, there were 80,756 objects in common with our G_M values and 133,884 objects for comparison with our G_B . The wide and oddly-shaped distribution of the difference in slope parameters between our MC technique and Oszkiewicz et al. (2012) (fig. 12) illustrates the difficulty and large uncertainty in measuring G .

Table 6: Slope parameters derived in this work (PS1: G_B , second column; G_M fifth column) and by Oszkiewicz et al. (2012) (OSK12: G_B , third column; G_M , sixth column) for the same objects in five different spectral classes. The fourth and last columns are the number of objects in common between the two data sets with SDSS spectral classification (Carvano et al., 2010).

Taxonomic Class	G_B PS1	G_B OSK12	N	G_M PS1	G_M OSK12	N
Q	0.21±0.28	0.20 ± 0.10	1324	0.46±0.53	0.54 ± 0.22	886
S	0.22±0.28	0.19 ± 0.22	14686	0.47±0.53	0.55 ± 0.20	10231
C	0.18±0.28	0.16 ± 0.10	7892	0.58±0.55	0.66 ± 0.23	5150
D	0.23±0.29	0.19 ± 0.12	1321	0.42±0.52	0.61 ± 0.25	852
X	0.19±0.28	0.18 ± 0.11	2073	0.53±0.54	0.59 ± 0.24	1428

The distribution peaks at zero for the B89 phase function with $\overline{G_B - G_{B,OSK}} = 0.00 \pm 0.01$ but there is a significant offset using the M10 phase function of $\overline{G_M - G_{M,OSK}} = -0.06 \pm 0.01$ (fig. 12). The RMS of the difference is larger using the M10 (0.58) than with the B89 phase function (0.35) but this is expected due to the numerically larger expected values of $G_M \sim 0.5$.

Fig. 12 also illustrates that our MC technique yields slope parameters that are comparable or marginally better than the work of Oszkiewicz et al. (2012), even though our data sample includes much less photometric data per object over a narrower phase angle range, presumably because of the Pan-STARRS1 system's superior photometry and the use of measured photometric uncertainties. The mean uncertainty for 80,756 objects in common with Oszkiewicz et al. (2012) is 0.33 ± 0.01 (RMS= 0.14) with our MC technique and is 0.39 ± 0.01 (RMS= 0.18) for the values reported by Oszkiewicz et al. (2012).

Slope parameters are taxonomy-dependent (Harris, 1989; Lagerkvist and Magnusson, 1990; Oszkiewicz et al., 2012; Pravec et al., 2012) but most of the objects in our Pan-STARRS1 data sample are fainter than known asteroids with well established taxonomies, so we relied on the SDSS spectral classification (Hasselmann et al., 2012) to assess our method's ability to detect the taxonomic-dependence. We found 48 asteroids in common with Pravec et al. (2012) and 18,541 with Oszkiewicz et al. (2012) (excluding values around $G_M \sim 0.20$) for which we could compare our calculated slope parameters. Our mean±RMS G_B values are consistent with Pravec et al. (2012) (Table 4.3) but our RMS distribution is much larger and the common number of asteroids is very low. Similarly, our G_B and G_M values (Table 6) are consistent Oszkiewicz et al. (2012) but the RMS distributions are large in both cases. There is a formal difference between the means of some of

the taxonomic classes but we do not consider them further because of the large uncertainties on each value and the large RMS of each taxonomic class' G distribution.

As discussed above in section 3.1, the phase curve coefficients G_B and G_M are functions of asteroid composition. Given the compositional trends of the inner belt being dominated by silicate S-type asteroids and carbon/volatile-rich asteroids in the outer belt, we should expect to see these trends reflected in our derived phase functions. A similar study was performed by Oszkiewicz et al. (2012) in their analysis of the MPC database. They found correlations between their measured G12 and orbital elements throughout the main belt, reflecting the general compositional gradient and family structure. To study this in our database we selected the 51,864 asteroids with orbital semi-major axes $2.1 \leq a \leq 3.3$ AU where the range of phase angles observed was $\Delta\alpha \geq 5^\circ$ and there were $N \geq 6$ observations. We then calculated the running median values $\overline{G_B}$ and $\overline{G_M}$ as a function of orbital a over a range $\Delta a = 0.05$ AU.

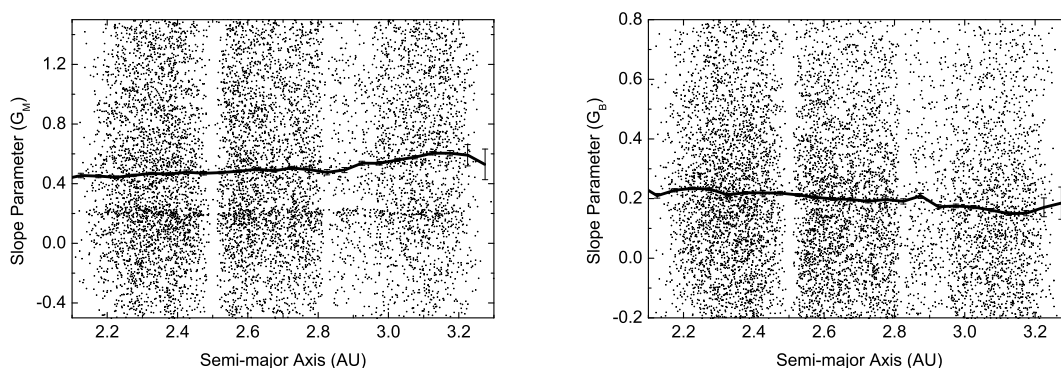


Figure 13: Moving average of G_M (top) and G_B (bottom) as a function semi-major axis.

Figure 13 clearly shows clear a negative trend in $\overline{G_B}$ and a positive trend in $\overline{G_M}$ with orbital a . As G_B is larger for S-type than C-type asteroids, while G_M becomes smaller, this agrees with the established compositional gradient in the main-belt. For modelling purposes, these trends may be approximated by the relationships $\overline{G_B} = -0.103a + 0.446$ and $\overline{G_M} = 0.237a - 0.175$ within the main belt. The largest deviations from these relationships occur at the 3:1 Kirkwood gap at 2.50 AU, and at the 7:3 gap at 2.95 AU. This latter position marks where the S-type asteroids of the dominant Koronis family of gives way to the T/X/K/D-type asteroids of the Eos family (Mothé-Diniz et al., 2005). We note that the overall observed scatter in individual values is dominated by ΔG , although it will also be partly due to the large amount of compositional mixing

present in the main belt (DeMeo and Carry, 2013).

5. Availability

The Pan-STARRS1 absolute magnitudes and slope parameters with associated uncertainties as described herein are available on-line (Appendix Appendix A). The eventual goal is that the catalog will be updated with all the data from the entire 3 year Pan-STARRS1 mission and then updated regularly with new data from the ongoing extended mission that is purely focused on the solar system. This effort will provide almost complete coverage of all known asteroids with extensive phase angle coverage and good number of detections per object.

6. Conclusions

Our work introduces a Monte Carlo method for calculating absolute magnitudes (H) and slope parameters (G) and their statistical uncertainties and systematic errors that is applicable to single apparition asteroid observations and designed to handle limited photometric data over a restricted phase angle range. The technique's utility was confirmed by comparing our H and G values to the well-established results of Pravec et al. (2012) for a limited number of objects. We then applied it to derive H and G with statistical uncertainties and systematic errors for $\sim 240,000$ numbered asteroids observed in the first 15 months of Pan-STARRS1's 3-year nominal mission. The single-survey data, consistent image processing, and well-defined photometric calibration, eliminates many of the problems encountered in past attempts to measure absolute magnitudes and slope parameters from a combination of different surveys.

We find that the Muinonen et al. (2010) phase function provides better results than the Bowell et al. (1989) phase function in terms of reducing the statistical uncertainty and systematic error on the absolute magnitude — both crucial to accurately predicting ephemeris apparent magnitudes and calculating asteroid albedos from H and measured asteroid diameters. There is a systematic H -dependent offset between the Minor Planet Center's reported absolute magnitude and H derived in this work with a maximum offset of about 0.25 mags at $H \sim 14$.

The measured slope parameters are generally in agreement with the results of Pravec et al. (2012) and Oszkiewicz et al. (2012) but the statistical uncertainty and systematic error on any individual asteroid's G is large due to poor temporal and phase-space coverage.

7. Acknowledgements

The Pan-STARRS1 Surveys have been made possible through contributions of the Institute for Astronomy, the University of Hawaii, the Pan-STARRS Project Office, the Max-Planck Society and its participating institutes, the Max Planck Institute for Astronomy, Heidelberg and the Max Planck Institute for Extraterrestrial Physics, Garching, The Johns Hopkins University, Durham University, the University of Edinburgh, Queen's University Belfast, the Harvard-Smithsonian Center for Astrophysics, and the Las Cumbres Observatory Global Telescope Network, Incorporated, the National Central University of Taiwan, and the National Aeronautics and Space Administration under Grant No. NNX08AR22G and No. NNX12AR65G issued through the Planetary Science Division of the NASA Science Mission Directorate.

Appendix A. Pan-STARRS1 asteroid database

Version 1.0 of the Pan-STARRS1 asteroid database is available at <http://www.ifa.hawaii.edu/NEO/>. It provides derived H and G values for 248,457 asteroids with a total of 1,242,282 detections spanning the time interval from February 2011 to May 2012 as described in this work. The 18 column data file is comma-delimited and each line represents a single asteroid. The columns are described in table A.7.

Table A.7: Pan-STARRS1 asteroid database v1.0 column descriptions.

Col. #	Col. value	Description
1	ID	The object's designation in the MPC's 5-character format. The MPC database is accessible online. ^a
2	class	The object's taxonomic class as specified by the Sloan Digital Sky Survey (Hasselmann et al., 2012) from the Planetary Data System, version 1.1, available online ^b . NULL if unknown.
3	N	number of detections used in the fit
4	$\Delta\alpha$	phase angle range
5	$H_{B,i}$	initial estimate of the absolute magnitude using the B89 phase curve
6	H_B	absolute magnitude derived using our MC technique in the B89 photometric system
7	δH_B	uncertainty on the absolute magnitude in col. 6
8	ΔH_B	estimated error on the absolute magnitude in col. 6
9	$H_{M,i}$	initial estimate of the absolute magnitude using the M10 phase curve
10	H_M	absolute magnitude derived using our MC technique with the M10 phase curve
11	δH_M	uncertainty on the absolute magnitude in col. 10
12	ΔH_M	estimated error on the absolute magnitude in col. 10
13	G_B	slope parameter derived using our MC technique in the B89 photometric system
14	δG_B	uncertainty on the slope parameter in col. 13
15	ΔG_B	estimated error on the slope parameter in col. 13
16	G_M	slope parameter derived using our MC technique in the M10 photometric system
17	δG_M	uncertainty on the slope parameter in col. 16
18	ΔG_M	estimated error on the slope parameter in col. 16

^a<http://www.minorplanetcenter.net/iau/MPCORB/MPCORB.DAT>

^b<http://sbn.psi.edu/pds/resource/sdsstax.html>

References

- Bowell, E., Hapke, B., Domingue, D., Lumme, K., Peltoniemi, J., Harris, A., 1989. In: Gehrels, T., Matthews, M. T., Binzel, R. P. (Eds.), *Asteroids III*. University of Arizona Press, Chapter Application of photometric models to asteroids, pp. 524–555.
- Carvano, J. M., Hasselmann, P. H., Lazzaro, D., Mothé-Diniz, T., 2010. SDSS-based taxonomic classification and orbital distribution of main belt asteroids. *aap510*, A43.
- de la Fuente Marcos, C., de la Fuente Marcos, R., 2013. A resonant family of dynamically cold small bodies in the near-Earth asteroid belt. *mnr434*, L1–L5.
- DeMeo, F. E., Carry, B., 2013. The taxonomic distribution of asteroids from multi-filter all-sky photometric surveys. *226* (1), 723–741.
- Denneau, L., Jedicke, R., Grav, T., Granvik, M., Kubica, J., Milani, A., Vereš, P., Wainscoat, R., Chang, D., Pierfederici, F., Kaiser, N., Chambers, K. C., Heasley, J. N., Magnier, E. A., Price, P. A., Myers, J., Kleyna, J., Hsieh, H., Farnocchia, D., Waters, C., Sweeney, W. H., Green, D., Bolin, B., Burgett, W. S., Morgan, J. S., Tonry, J. L., Hodapp, K. W., Chastel, S., Chesley, S., Fitzsimmons, A., Holman, M., Spahr, T., Tholen, D., Williams, G. V., Abe, S., Armstrong, J. D., Bressi, T. H., Holmes, R., Lister, T., McMillan, R. S., Micheli, M., Ryan, E. V., Ryan, W. H., Scotti, J. V., 2013. The Pan-STARRS Moving Object Processing System. *pasp125*, 357–395.
- Fukugita, M., Ichikawa, T., Gunn, J. E., Doi, M., Shimasaku, K., Schneider, D. P., 1996. The Sloan Digital Sky Survey Photometric System. *aj111*, 1748.
- Grav, T., Mainzer, A. K., Bauer, J., Masiero, J., Spahr, T., McMillan, R. S., Walker, R., Cutri, R., Wright, E., Eisenhardt, P. R., Blauvelt, E., DeBaun, E., Elsbury, D., Gautier, T., Gomillion, S., Hand, E., Wilkins, A., 2012. WISE/NEOWISE Observations of the Hilda Population: Preliminary Results. *Astrophysical Journal* 744, 197.
- Grav, T., Mainzer, A. K., Bauer, J. M., Masiero, J. R., Nugent, C. R., 2012. WISE/NEOWISE Observations of the Jovian Trojan Population: Taxonomy. *Astrophysical Journal* 759, 49.
- Harris, A. W., 1989. The H-G Asteroid Magnitude System: Mean Slope Parameters. In: Lunar and Planetary Institute Science Conference Abstracts, Volume 20 of *Lunar and Planetary Inst. Technical Report*, pp. 375.

- Hasselmann, P., Carvano, J. M., Lazzaro, D., 2012. Sdss-based asteroid taxonomy v1.1. ear-a-i0035-5-sdsstax-v1.1.
- Holsapple, K. A., 2007. Spin limits of Solar System bodies: From the small fast-rotators to 2003 EL61. *Icarus* 187, 500–509.
- Jedicke, R., Larsen, J., Spahr, T., 2002. Observational Selection Effects in Asteroid Surveys. *Asteroids III*, 71–87.
- Jurić, M., Ivezić, Ž., Lupton, R. H., Quinn, T., Tabachnik, S., Fan, X., Gunn, J. E., Hennesy, G. S., Knapp, G. R., Munn, J. A., Pier, J. R., Rockosi, C. M., Schneider, D. P., Brinkmann, J., Csabai, I., Fukugita, M., 2002. Comparison of Positions and Magnitudes of Asteroids Observed in the Sloan Digital Sky Survey with Those Predicted for Known Asteroids. *Astronomical Journal* 124, 1776–1787.
- Kaiser, N., Burgett, W., Chambers, K., Denneau, L., Heasley, J., Jedicke, R., Magnier, E., Morgan, J., Onaka, P., Tonry, J., 2010. The pan-starrs wide-field optical/nir imaging survey. In: Stepp L.M., G. R., H.J., H. (Eds.), *Ground-based and Airborne Telescopes III, Volume 7732 of Proceedings of the SPIE*, pp. 77330E–77330E–14.
- Lagerkvist, C.-I., Magnusson, P., 1990. Analysis of asteroid lightcurves. II - Phase curves in a generalized HG-system. *Astronomy and Astrophysics, Supplement* 86, 119–165.
- Law, N. M., Kulkarni, S. R., Dekany, R. G., Ofek, E. O., Quimby, R. M., Nugent, P. E., Surace, J., Grillmair, C. C., Bloom, J. S., Kasliwal, M. M., Bildsten, L., Brown, T., Cenko, S. B., Ciardi, D., Croner, E., Djorgovski, S. G., van Eyken, J., Filippenko, A. V., Fox, D. B., Gal-Yam, A., Hale, D., Hamam, N., Helou, G., Henning, J., Howell, D. A., Jacobsen, J., Laher, R., Mattingly, S., McKenna, D., Pickles, A., Poznanski, D., Rahmer, G., Rau, A., Rosing, W., Shara, M., Smith, R., Starr, D., Sullivan, M., Velur, V., Walters, R., Zolkower, J., 2009. The Palomar Transient Factory: System Overview, Performance, and First Results. *pasp121*, 1395–1408.
- Levenberg, K., 1944. A method for the solution of certain problems in least squares. *Quarterly of Applied Mathematics* 2, 164–168.
- Lupton, R., 2007. The characterization, subtraction, and addition of astronomical images. In: G.J., B., E.D., F. (Eds.), *Statistical Challenges in Modern Astronomy IV, Volume 371 of ASP Conference Series*, pp. 160–172.

- Magnier, E., 2006. The Pan-STARRS PS1 Image Processing Pipeline. In: The Advanced Maui Optical and Space Surveillance Technologies Conference.
- Magnier, E. A., Schlafly, E., Finkbeiner, D., Juric, M., Tonry, J. L., Burgett, W. S., Chambers, K. C., Flewelling, H. A., Kaiser, N., Kudritzki, R.-P., Morgan, J. S., Price, P. A., Sweeney, W. E., Stubbs, C. W., 2013. The Pan-STARRS 1 Photometric Reference Ladder, Release 12.01. *Astrophysical Journal*, Supplement 205, 20.
- Marquardt, D., 1963. An algorithm for least-squares estimation of nonlinear parameters. *SIAM Journal on Applied Mathematics* 11, 431–441.
- Masiero, J., Jedicke, R., Ďurech, J., Gwyn, S., Denneau, L., Larsen, J., 2009. The Thousand Asteroid Light Curve Survey. *Icarus* 204, 145–171.
- Milani, A., Gronchi, G. F., Farnocchia, D., Knežević, Z., Jedicke, R., Denneau, L., Pierfederici, F., 2008. Topocentric orbit determination: Algorithms for the next generation surveys. *Icarus* 195, 474–492.
- Mothé-Diniz, T., Carvano, J. M. Á., Lazzaro, D., 2003. Distribution of taxonomic classes in the main belt of asteroids. *Icarus* 162, 10–21.
- Mothé-Diniz, T., Roig, F., Carvano, J. M., 2005. Reanalysis of asteroid families structure through visible spectroscopy. *Icarus* 174 (1), 54–80.
- Muironen, K., Belskaya, I., Cellino, A., Delbo, M., Levasseur-Regourd, A.-C., Penttilä, A., Tedesco, E., 2010. A three-parameter magnitude phase function for asteroids. *Icarus* 209, 542–555.
- Oszkiewicz, D. A., Bowell, E., Wasserman, L. H., Muironen, K., Penttilä, A., Pieniluoma, T., Trilling, D. E., Thomas, C. A., 2012. Asteroid taxonomic signatures from photometric phase curves. *Icarus* 219, 283–296.
- Pravec, P., Harris, A. W., Kušnirák, P., Galád, A., & Hornoch, K. 2012, *Icarus* , 221, 365
- Schlafly, E. F., Finkbeiner, D. P., Jurić, M., Magnier, E. A., Burgett, W. S., Chambers, K. C., Grav, T., Hodapp, K. W., Kaiser, N., Kudritzki, R.-P., Martin, N. F., Morgan, J. S., Price, P. A., Rix, H.-W., Stubbs, C. W., Tonry, J. L., Wainscoat, R. J., 2012. Photometric Calibration of the First 1.5 Years of the Pan-STARRS1 Survey. *Astrophysical Journal* 756, 158.

- Stuart, J. S., Binzel, R. P., 2004. Bias-corrected population, size distribution, and impact hazard for the near-Earth objects. *Icarus* 170, 295–311.
- Tonry, J., Onaka, P., 2009. The Pan-STARRS Gigapixel Camera. In: *Advanced Maui Optical and Space Surveillance Technologies Conference*.
- Tonry, J. L., Stubbs, C. W., Lykke, K. R., Doherty, P., Shivvers, I. S., Burgett, W. S., Chambers, K. C., Hodapp, K. W., Kaiser, N., Kudritzki, R.-P., Magnier, E. A., Morgan, J. S., Price, P. A., Wainscoat, R. J., 2012. The Pan-STARRS1 Photometric System. *Astrophysical Journal* 750, 99.
- Warner, B. D., Harris, A. W., Pravec, P., 2009. The asteroid lightcurve database. *Icarus* 202, 134–146.
- Waszczak, A., Chang, C.-K., Ofek, E. O., Laher, R., Masci, F., Levitan, D., Surace, J., Cheng, Y.-C., Ip, W.-H., Kinoshita, D., Helou, G., Prince, T. A., Kulkarni, S., 2015. Asteroid lightcurves from the Palomar Transient Factory survey: Rotation periods and phase functions from sparse photometry. *ArXiv e-prints*.
- Wiegert, P. A., Innanen, K. A., Mikkola, S., 1997. An asteroidal companion to the Earth. *Nature* 387, 685–686.
- Zavodny, M., Jedicke, R., Beshore, E. C., Bernardi, F., Larson, S., 2008. The orbit and size distribution of small Solar System objects orbiting the Sun interior to the Earth's orbit. *Icarus* 198, 284–293.